SOFT ROBOTICS
Volume 00, Number 00, 2021

DOI: 10.1089/soro.2020.0207

SoRo
Soft Robotics

Stiffness Preprogrammable Soft Bending Pneumatic Actuators for High-Efficient, Conformal Operation

Xingxing Ke,[1] Jiajun Jang,[1] Zhiping Chai,[1] Haochen Yong,[1] Jiaqi Zhu,[1] Han Chen,[1] Chuan Fei Guo,[2] Han Ding,[1] and Zhigang Wu[1]

Abstract

Soft pneumatic actuators (SPAs) are extensively investigated due to their simple control strategies for producing sophisticated motions. However, the motions or operations of homogeneous SPAs show obvious limitations in some varying curvature interaction scenarios because of the profile mismatch of homogeneous SPAs and specific interacted objects. Herein, a stiffness preprogrammable soft pneumatic actuator (SPSPA) is proposed by discretely presetting gradient geometrical or materials distributions. Through finite element analysis and experimental validation, a mathematical model of behavior prediction of SPSPA was built to relate the geometrical parameters/materials with its morphing behaviors, making it possible to reversely obtain designed parameters. This design strategy enables conformal and efficient interaction in some curvature varying scenarios. Specifically, higher effective contact area, perimeter utilization ratio, and conformal ability can be obtained while interacting with those inhomogeneous curvature objects, for example, more than 434.7% improvement in contact area rates and 12.5% enhancement in perimeter utilization ratios toward a typical equilateral triangle object. Further, a serial of SPSPAs that have conformal grasping/interactive capability, better contact sensing behaviors were demonstrated. For example, an SPSPA and an SPSP robot were demonstrated, which showed better kinetic, kinematic characterizations and sensing capability compared with the homogeneous one while coming across varying curvature objects. Moreover, underactuated finger rehabilitation SPSPAs were demonstrated with customized profiles and coupled joint motion. This customized scheme can be potentially used in those specific-purposed, single, and repetitive application scenarios where varying curvature, conformal and efficient interaction are needed.

Keywords: stiffness preprogrammable structures, soft bending actuators, variable curvature actuators, finger rehabilitation

Introduction

The development of soft pneumatic actuators (SPAs) has made many new motions, such as bending, extending, and twisting, possible, and it achieves a series of dexterous locomotion or grabbing tasks.[1,2] This kind of actuators utilize large deformation from soft materials and structure, showing previous inaccessible flexibilities, compliance, and adaptabilities, when compared with their conventional rigid counterparts.[3–7] These actuations further broaden the robot application boundaries in recent developments, for example, compliant grabbing, flexible locomotion, bioinspired adhesion, dynamic camouflage, and other complex and nonlinear behaviors.[8–12] Also, inheriting the natural advantages of soft materials, it can operate in a biocompatible and interactive way in many scenarios, especially in those biomedicine, human–machine interaction, and ultrafine or collaborative operation unstructured scenarios.[13–16]

Enormous progress has been made in the soft robot development based on pneumatic principles in the past decades, showing abundant motion capability,[17–21] for example, prior work by Verma *et al.* developed a soft tube-climbing robot

[1]State Key Laboratory of Digital Manufacturing Equipment and Technology, Huazhong University of Science and Technology, Wuhan, China.
[2]Department of Materials Science and Engineering, Southern University of Science and Technology, Shenzhen, China.

driven by vacuum, which can navigate through a tube with turns, inclines, and varying diameters.[22] Similarly, Shepherd *et al.* reported a multigait soft robot, where a combination of crawling and undulation gaits allow it to navigate through a challenge obstacle.[1] Recently, the response characteristics can be programmed via structural parameters or materials properties, for example, a three-dimensional (3D) printed soft actuator with programmable bioinspired architecture.[23] In addition, a bio-inspired conformal and helical soft fabric gripper with variable stiffness and touch sensing was developed, showing versatile gripping capabilities.[24] However, for most presented pneumatic actuators, the single actuators always show a relatively homogeneous deformation behavior that cannot conform well in morphology, especially for those nonlinear scenarios (Fig. 1A). This mismatching of interaction interface significantly hinders high-efficient and compatible motions and interactions of soft robots, for example, precise operations, contacting sensing, and human–machine interaction. Recently, via additional programmable fabric constraints, several preprogramming SPA design methods have been developed.[25,26] Nevertheless, integral design approaches that can directly preset stiffness profiles into body structure without other additional fabric constraints to achieve an addressable behavior in single actuator are rarely studied. Therefore, to fully exploit the operation and interaction potential of SPAs in those specific-purposed, single, and repetitive application scenarios where varying curvature, conformal and efficient interaction are needed, it is necessary to seek new design principles that are capable of generating nonlinear addressable responding actuators in a facile and robust way.

Preprogramming in structure dimensions and materials distribution is a widely used strategy for achieving programmable behavior.[25,27–30] This endows constructed structures with customizable response behaviors under a homogeneous external or internal stimulus. For instance, a grayscale 3D printing method for graded materials with a widely tunable mechanical gradient was reported, and tailored functional gradients were achieved.[31] Meanwhile, a programmable tensegrity for soft robotics was developed, and the system-level mechanics in a soft structure can be programmed with various design parameters to achieve specific mechanic behaviors.[32] Similarly, using origami tessellations, Dudte *et al.* showed that scale-independent elementary geometric constructions and constrained optimization algorithms can be used to determine spatially modulated patterns that yield approximations to given surfaces of constant or varying curvature, which enables the tailoring of origami patterns to drape complex surfaces independent of absolute scale.[33] Previously, our group also developed a method for a seamless transition between heterogeneous moduli parts made of polydimethylsiloxane (PDMS)-based elastomer.[34,35] These tailored structures show addressable morphing and can fit the target shapes with better conformability, due to varying material properties or gradated mechanical structures. Despite the impressive achievements, research on integral, addressable morphing SPAs is rare, and a facile, flexible design route and corresponding reversal solution method are required urgently for better robotic operations and interactions.

Herein, to explore better operations and interactions in varying curvature scenarios, a stiffness preprogrammable soft pneumatic actuator (SPSPA) was proposed via encoding the structural parameters and materials (Fig. 1B). The influence of several critical parameters on its morphing characteristics has been systematically studied, and a predication model relating these parameters with its morphing shape is built. It enables customizable morphing behaviors of SPAs for specific operations and interaction demands, addressing the mismatching of the interaction interface. Based on this method, a remarkable increment of contact ratio and a certain improvement of perimeter utilization ratio were achieved toward the grasping of several typical shaped objects. Further, several SPSPAs were tailored for conformal grasping and contact sensing, for example, grasping a triangular-like cake and contact scanning crack on a varying curvature blade, which shows a conformal and effective interaction with these specific shaped objects. Moreover, a soft crawling robot

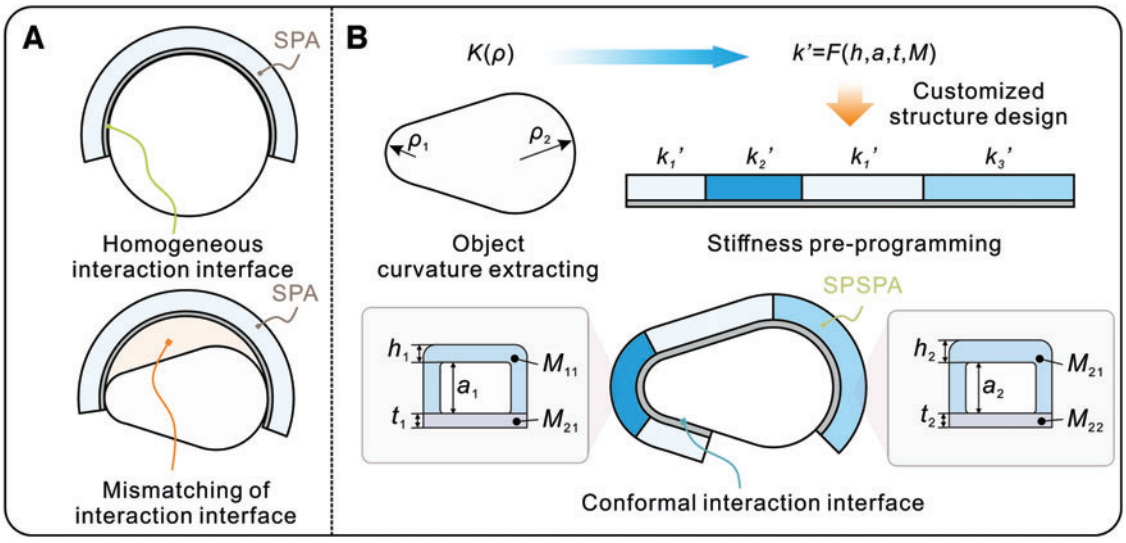

FIG. 1. Concept of SPSPA. **(A)** Homogeneous SPA producing a mismatching between interaction interfaces in some inhomogeneous scenarios. **(B)** SPSPA design for conformal interaction. SPA, soft pneumatic actuator; SPSPA, stiffness preprogrammed soft pneumatic actuator. Color images are available online.

integrated with SPSPAs was demonstrated, showing superior kinetic and kinematic characteristics over a homogeneous one. Further, underactuated finger rehabilitation SPSPAs (FR-SPSPAs) are demonstrated with conformal morphing and coupled knuckle motions. This customizable design method may offer a useful route for conformal, gentle, and high-efficient robotic operation and sensing interaction, for example, gentle rehabilitation interaction, conformal sensing, and compatible manipulation of tender/fragile objects. Meanwhile, it can also significantly simplify the complexity of actuation and control leveraging inherent physical intelligence.

Materials and Methods

Design of SPSPAs

The responsive behaviors of actuators highly depend on their structure stiffness, and here a structure stiffness presetting method is proposed for designing SPSPAs. Herein, to describe the local bending stiffness of an actuator, an equivalent stiffness (k') was defined as $k' = p/w$ (where p is the actuation pressure, w is the deflection). As shown in Figure 1, via selective presetting and tuning the geometrical dimensions and materials, a targeted shaped responsive actuator can be obtained. More details are shown in Figure 2A: (1) obtaining the shape profiles of the targeted/interacted object; (2) extracting the curvature profiles of the targeted shape; (3) calculating the equivalent stiffness profiles of the actuator; (4) inversely solving the structural or material parameters according to the calculated stiffness distribution; (5) designing a corresponding fabrication mold according to the solved parameters (detailed designed protocols are in Supplementary Data).

Fabrication

Details for the fabrication of the soft actuators and robots are shown in Figure 2B. Briefly, we fabricated the robot leveraging soft lithography method.[1] Specifically, we used a 3D printer to print the mold where the soft actuators and robots were replicated. The structural parameters can be predesigned in the mold to preset the bending structural stiffness of actuators. We used Ecoflex 00-10, 00-30, and 00-50 (Smooth-On) as the stretchable layer materials and PDMS elastomer (Sylgard184; Dow Corning,) with different mixture ratios as the limiting layer materials. The stretchable layer and the limiting layer were bonded by silicone rubber adhesive (Sil-poxy; Smooth-On).

Operation and characteristics

The soft actuators and robots were actuated by a self-developed automatic actuated system or a manual actuation manner by multiple syringes (Supplementary Fig. S1). We quantified the response characteristics of soft robots using a digital camera (Canon EOS 70D; Tokyo, Japan) to track their positions and record their morphing profiles. The profile was analyzed and extracted by the image morphology method in MATLAB 2019a. The input gas pressure was measured with a digital pressure gauge (MIK-Y190; Asmik). The output pull force was quantified by a force sensor (model 3131; Arizon) with a data acquisition unit (FD0823; Arizon) with 30 Hz sampling frequency. FR-SPSPAs were made of biocompatible, non-instrusive and medically licensed rubber with gentle force output that would have almost no effect on the human body. The volunteer was one of our healthy coauthor, and the whole rehabilitation process is fully noticed by the volunteer and approved by all authors.

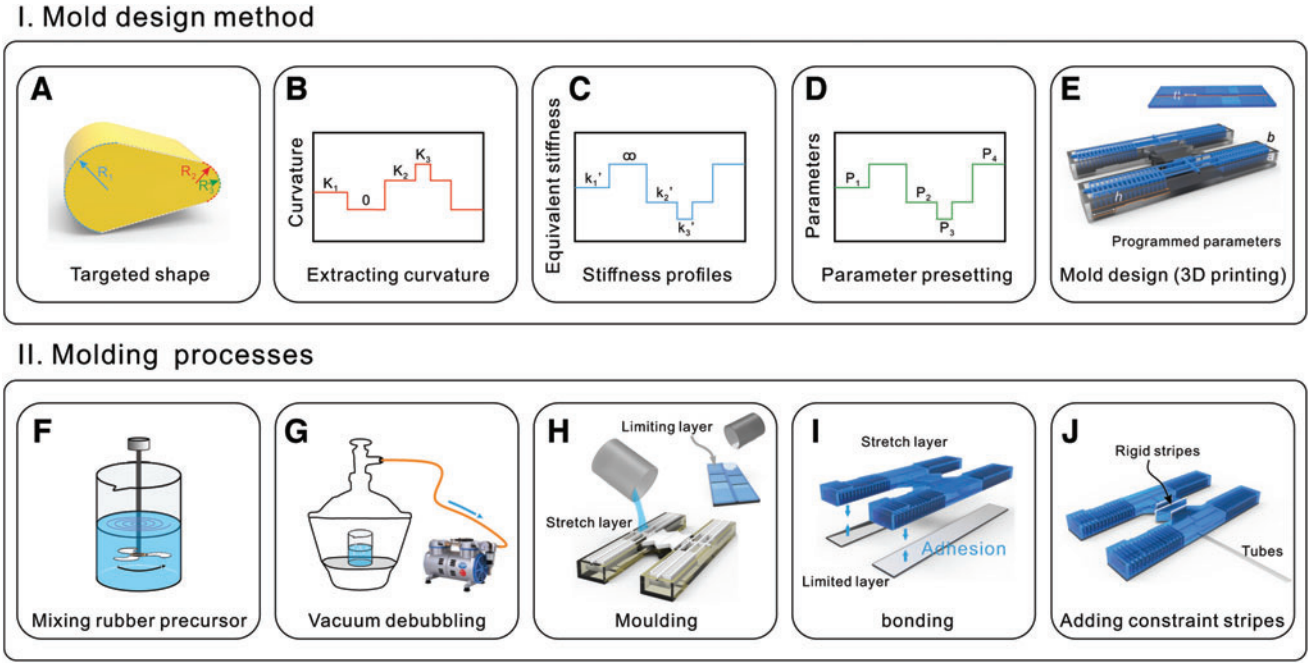

FIG. 2. Design and fabrication processes. **(A)** Obtaining the shape of targeted object. **(B)** Extracting the profile curvature. **(C)** Calculating the stiffness profiles of the bending actuator. **(D)** Inversely solving the structural or materials parameters according to calculated stiffness distribution. **(E)** Designing corresponding fabrication mold according to the solved parameters. **(F)** Mixing rubber precursor. **(G)** Removing bubbles in a vacuum vessel. **(H)** Molding robots by casting rubber precursor into the designed mold. **(I, J)** Bonding the stretchable layer and limiting layer with silicone rubber adhesive. Color images are available online.

Finite element analysis

For simulation results presented in corresponding sections, we carried out nonlinear finite element analyses in Abaqus 6.14. Experimental stress–strain data for different types of Ecoflex and PDMS of different mixture ratios were utilized for curve fitting using the built-in-fitting tool by the least-square method in COMSOL CAE 5.2a. Assuming incompressibility, appropriate strain energy functions (Mooney-Rivlin for PDMS, Yeoh for Ecoflex) were selected based on model stability and closeness of fit (details in Supplementary Notes). The model parameters are shown in Supplementary Tables S1 and S2. The uniformly distributed pressure is loaded on the internal chamber to equal the actuation pressure.

Results and Discussion

Mechanical investigations

For a pneumatic elastomer actuator, the materials will deform dramatically under the actuated process. Structural parameters and material properties play important roles in its bending stiffness and morphing behaviors. To systematically study and characterize the bending stiffness and morphing behaviors, here, a typical bending actuator is designed (Fig. 3A). Several critical structural parameters and various materials that will influence the behaviors of this kind of actuators are chosen. They are the top stretchable layer thickness h, the limiting layer thickness t, the internal cross-sectional height a, the stretchable layer materials, and limiting layer materials, respectively. A deflection defined as w quantitatively describes the response characteristics. By varying these critical variables, we systematically study their influential rules on the equivalent stiffness k' (defined as $k' = p/w$) of the soft bending actuator via a finite element analysis (FEA) method.

The bending morphing of the soft bending actuator is essentially a form of competitive behavior of asymmetric strain under a certain pressure load. The higher relative strain between the top stretchable layer and the bottom limiting layer will lead to a larger bending deformation. Particularly, the limiting layer produces a finite tensile deformation under the actuation process due to its relatively large elasticity modulus. Consequently, the stretchable layer thickness directly restrains the stretch deformation of the top layer during the actuation process. Therefore, the stretchable layer thickness plays a significant role in tuning the bending stiffness. According to the FEA results, with a thicker stretchable layer,

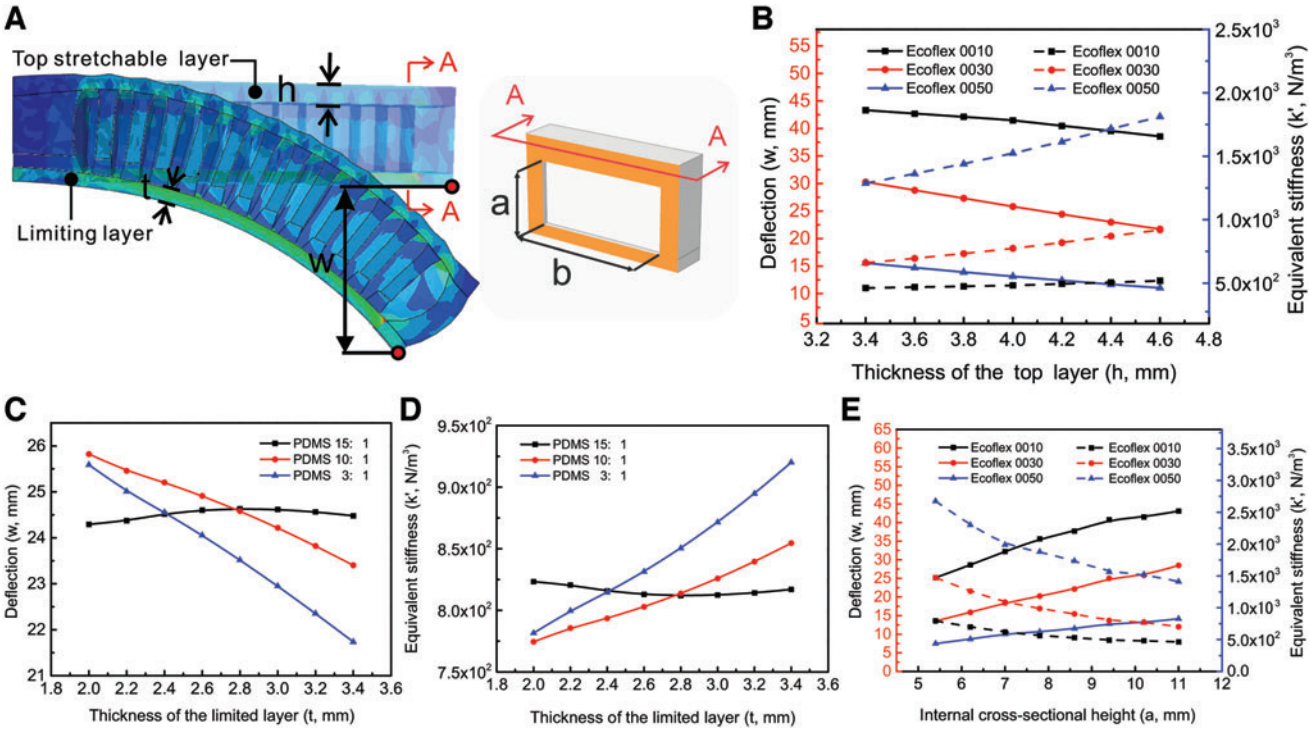

FIG. 3. Response characteristics of the bending actuator. **(A)** The structure of a bending actuator composed of a top stretchable layer and a limiting layer. The structural parameters are defined as follows: the top stretchable layer thickness h, the limiting layer thickness t, and the chamber cross-section height a and width b, respectively. The response deflection is defined as w. **(B)** The response characteristics of the bending actuator with different thickness of the top layer (h) and different stretchable layer materials while the limiting layer is the 2.0 mm PDMS with the ratio of 10:1 under 20 kPa actuation pressure. Cross-sectional height a remains 10.2 mm, and b keeps 21 mm. **(C, D)** The response characteristics of the bending actuator, where the stretchable layer is the 4.0 mm Ecoflex 00-30, with different thicknesses of the limiting layer (t) and different limiting layer materials under 20 kPa actuation pressure. Cross-sectional height a remains 10.2 mm, and b keeps 21 mm. **(E)** The response characteristics of the bending actuator, where limiting layer is the 2.0 mm PDMS with the ratio of 10:1, with different chamber cross-section height a and different stretchable layer materials under 20 kPa actuation pressure. Thickness of top layer h remains 4 mm, and b keeps 21 mm. PDMS, polydimethylsiloxane. Color images are available online.

the bending actuator will show a larger stiffness and needs more actuated pneumatic pressure with the same limiting layer (Fig. 3B). Similarly, the material of the stretchable layer will influence the structural stiffness. According to the FEA results, with the larger material modulus, the bending actuator will be stiffer to bend as well.

Meanwhile, the limiting layer will also influence the response behaviors of the soft bending actuator, since the limiting layer with a greater elasticity modulus possesses a larger bending deformation and less tensile strain of the limiting layer. As shown in Figure 3C and D, the quantitative effect of the thickness and materials with a various modulus of the limiting layer on the deflection and the equivalent stiffness has been studied. We found that with a stiffer and thicker PDMS limiting layer, the bending actuator will obtain a larger equivalent stiffness with the same stretchable layer (Ecoflex 0030 with same structural parameters). Nevertheless, too large a ratio (weight ratio of PDMS base to cross-linker) and too thin a thickness of the PDMS limiting layer will weaken deflection response since the PDMS limiting layer will also produce relatively large tensile deformation, which reduces bilayer relative anisotropic strain. In addition, the internal cross-section parameters have also been explored, and this influence on similar actuators has been proved by previous work.[36] Here, the internal cross-sectional height a has been discussed since it will influence the bending moment. As shown in Figure 3E, with the increment of a, the soft bending actuator will obtain smaller equivalent stiffness, indicating that larger a makes the actuator easier to bend under the same actuation pressure in this discussion range of a. However, this parameter is not suitable for local stiffness programming since it is a global impact variable.

Modeling and experimental validations

To establish a model between the parameters and targeted curvature, an easily controlled and the most significant parameter is chosen for modeling. By numerical fitting, the relationship between equivalent stiffness and stretch thickness can be expressed as:

$$k' = \begin{cases} 47.22h + 297.64 & (\text{Ecoflex } 00-10) \\ 217.89h - 87.52 & (\text{Ecoflex } 00-30) \\ 439.94h - 223.45 & (\text{Ecoflex } 00-50) \end{cases} \quad (1)$$

where h is the stretchable layer thickness, and k' is the equivalent stiffness. As shown in Figure 4A, to relate the stiffness with the curvature radius of the actuator under a certain actuation pressure, curvature radius and deflection can be related by a geometrical relationship. The corresponding equation is as follows:

$$\begin{cases} \rho\cos\theta + w = \rho \quad (0^\circ < \theta < 180^\circ) & (2) \\ \rho\theta = L & (3) \\ k' = p/w & (4) \\ \rho = 1/K & (5) \end{cases}$$

where ρ is the curvature radius, θ is the central angle, p is the actuation pressure, L is the length of the limiting layer, and K is the curvature. The following equations are derived according to the earlier equations:

$$\rho\cos(L/\rho) + p/k' = \rho \quad (0^\circ < \theta < 180^\circ) \quad (6)$$

$$(1/K)\cos(LK) + p/k' = 1/K \quad (0^\circ < \theta < 180^\circ) \quad (7)$$

Substituting the constants into the earlier equations, where $L = 56.3$ mm, $p = 20{,}000$ Pa, the corresponding functions are shown in Figure 4B.

$$\rho\cos(56.3/\rho) + 20000/k' = \rho \ (\rho > 17.92\ mm) \quad (8)$$

$$(1/K)\cos(56.3K) + 20000/k' = 1/K \ (K < 0.056\ mm^{-1}) \quad (9)$$

According to the earlier equations, the targeted curvature and radius can be obtained by inputting appropriate structural dimensions and stretchable layer materials. Also, structural dimensions and stretchable layer materials can be inversely solved according to targeted curvature profiles. It offers a mathematical model for guiding the design of a specific curvature actuator.

To verify the derived model, a bending actuator with a curvature radius of 60 mm was selected as a design target. As shown in Figure 4C, two bending actuators were designed for targeted curvature with different stretchable layer material and geometrical dimensions according to the presented model. Two corresponding experimental bending actuators for designed targeted curvature were tested in Figure 4D and F, respectively (where Ecoflex 00-30 was employed as the stretchable layer materials in Fig. 4D, and Ecoflex 00-50 was employed as the stretchable layer materials in Fig. 4F). The actuation pressure for the former was 17.3 kPa for achieving the targeted curvature radius of 60 mm, and the latter was 17.9 kPa for achieving the same curvature radius. The limiting layer contours of two bending actuators were almost in keeping with the theoretical contour (Fig. 4F), and actuation pressure errors are 13.5% and 10.5% (the theoretical actuation is 20 kPa), respectively.

The earlier design model provides a method and route to accurately preset the stiffness distribution in a bending actuator and hence to influence its response and morphing behaviors. The design principles can be generally summarized as follows: The internal-cross sectional height can program the bending actuator into an appropriate desirable range in a global manner. Also, by local programming of the thickness and materials of the stretchable layer and limiting layer, respectively, the local stiffness can be preset in a desirable position in a local addressable manner. Consequently, an optimal structure can be obtained by preprogramming and conform to various object contours with varying curvature.

Adaptability investigations

To quantitatively characterize the adaptability of SPSPAs compared with those homogeneous actuators, several typical shaped objects with varying curvature were selected for comparisons by an FEA method (Fig. 5 and Supplementary Video S1), for example, to grab a triangular-like object, a homogeneous actuator and an SPSPA with the same length were designed (Fig. 5A–D). The SPSPA can achieve a better grasping toward this object in a more conformal way, compared with the homogeneous one. Specifically, as shown in

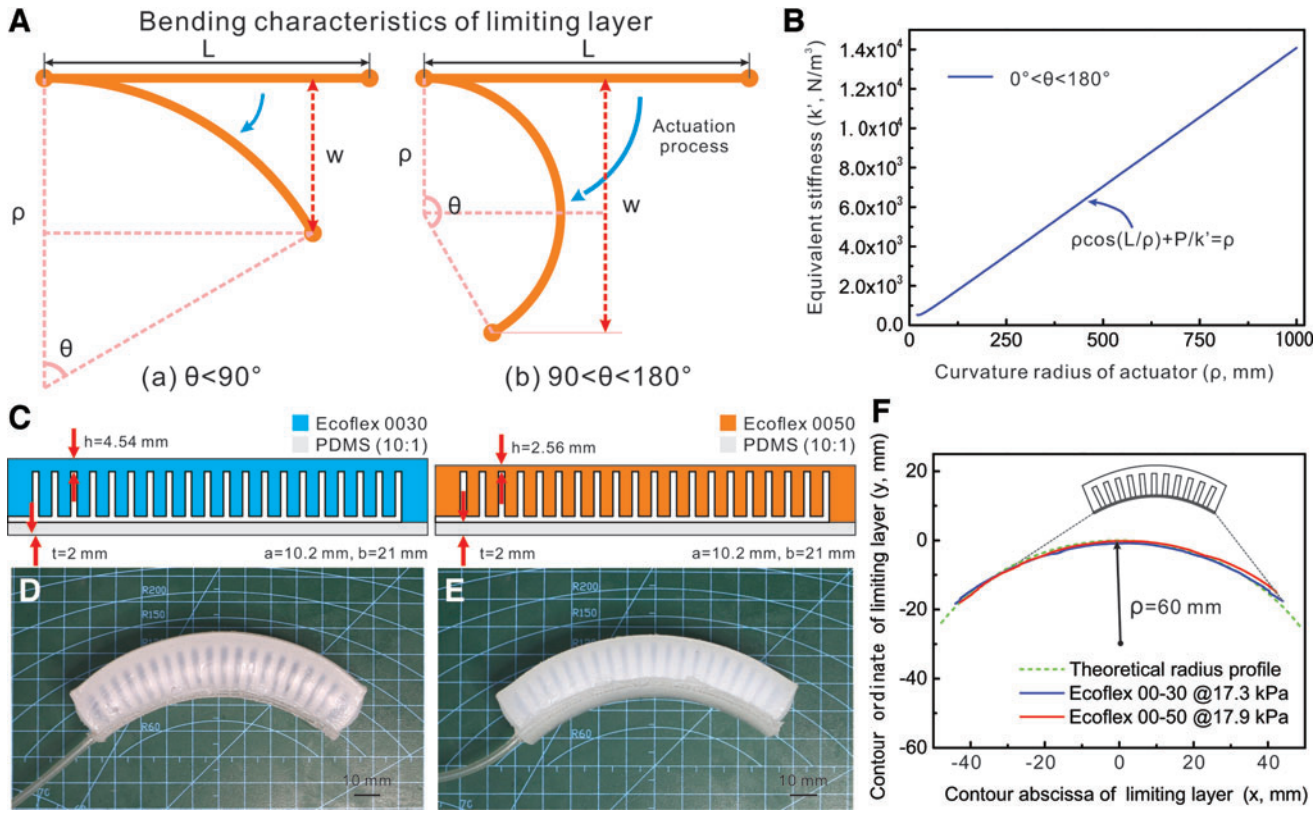

FIG. 4. Modeling morphing behaviors of the soft bending actuators. **(A)** The geometric relationship of the limiting layer profile under different bending angles. **(B)** Model predictions of the curvature radius of actuators with different equivalent stiffness under 20 kPa actuation pressure. **(C)** Two bending actuator structures with a designed curvature radius of 60 mm with different stretchable layer materials. **(D, E)** Experimental figures of two morphing actuators under the 17.3 and 17.9 kPa actuated pressure, respectively. **(F)** The limiting layer contour comparison of two actuators and the theoretical one. Color images are available online.

Figure 5E, the contact area ratio ($S_{contact}/S_{total}$) and perimeter coverage ratio ($C_{contact}/C_{total}$) were compared toward five typical shaped cases. Effective contact rates have been significantly increased and the perimeter utilization rates have been enhanced to a certain extent by employing the stiffness preprogrammed method, for example, more than 316.5%, 434.7%, 428.8%, 121.1%, and 137.8% improvement in contact area rates and 16.9%, 12.5%, 3.6%, 11.1%, and 15% enhancement in perimeter utilization ratios toward five typical shaped objects, respectively. Higher effective contact rates ensure better conformal grasping, which alleviates stress concentration and makes interaction with objects safer and steadier. Meanwhile, the higher perimeter coverage ratio makes the actuators more fully used in length. The simulation comparison of the other four cases in Figure 5E is shown in Figure 5F (the detailed designs are shown in Supplementary Fig. S2, and fabrication methods of multi-material SPSPAs are shown in Supplementary Fig. S3). The enhancement of these critical indexes ensures a conformal, effective interaction for some varying curvature scenarios.

Conformal demonstrations of SPSPAs

Here, several SPSPAs actuators were designed for specific application scenarios to demonstrate conformal grasping and interaction. As shown in Figure 6A, to adaptively attach to a varying curvature object, we made a soft embracing module designed according to the FEA results. The soft embracing module can conform to this varying curvature structure well at about 3.1 kPa actuation pressure, which is in good agreement with the simulation results within the specified tolerance range. Also, the response inhomogeneous morphing behavior of the soft embracing module has been characterized under the increasing actuated pressure (Fig. 6B). Since gravity will have a different influence on the morphing processes with different posture and fixed constraints, here, only the influences of pressure on response of the SPSPA are studied. To eliminate the influence of gravity on the deformation of the actuator, the soft embracing module was horizontally floating on the water surface to balance its gravity (test setup is in Supplementary Fig. S4). For practical use, gravity should be considered according to the specific condition. The profile of the soft embracing module shows an inhomogeneous morphing due to the preprogrammed structural parameters. In addition, to grasp a soft triangular cake, an SPSPA and a homogeneous actuator were designed (Fig. 6C–F), respectively. The preprogrammed actuator can achieve conformal and gentle grasping, as shown in Supplementary Video S2.

Further, contact sensing that was enabled by this conformal interaction has also been explored (Fig. 6G–L). To detect cracks on a varying curvature blade, a piezocapacitive sensor combined a pyramid-like structure was integrated on the

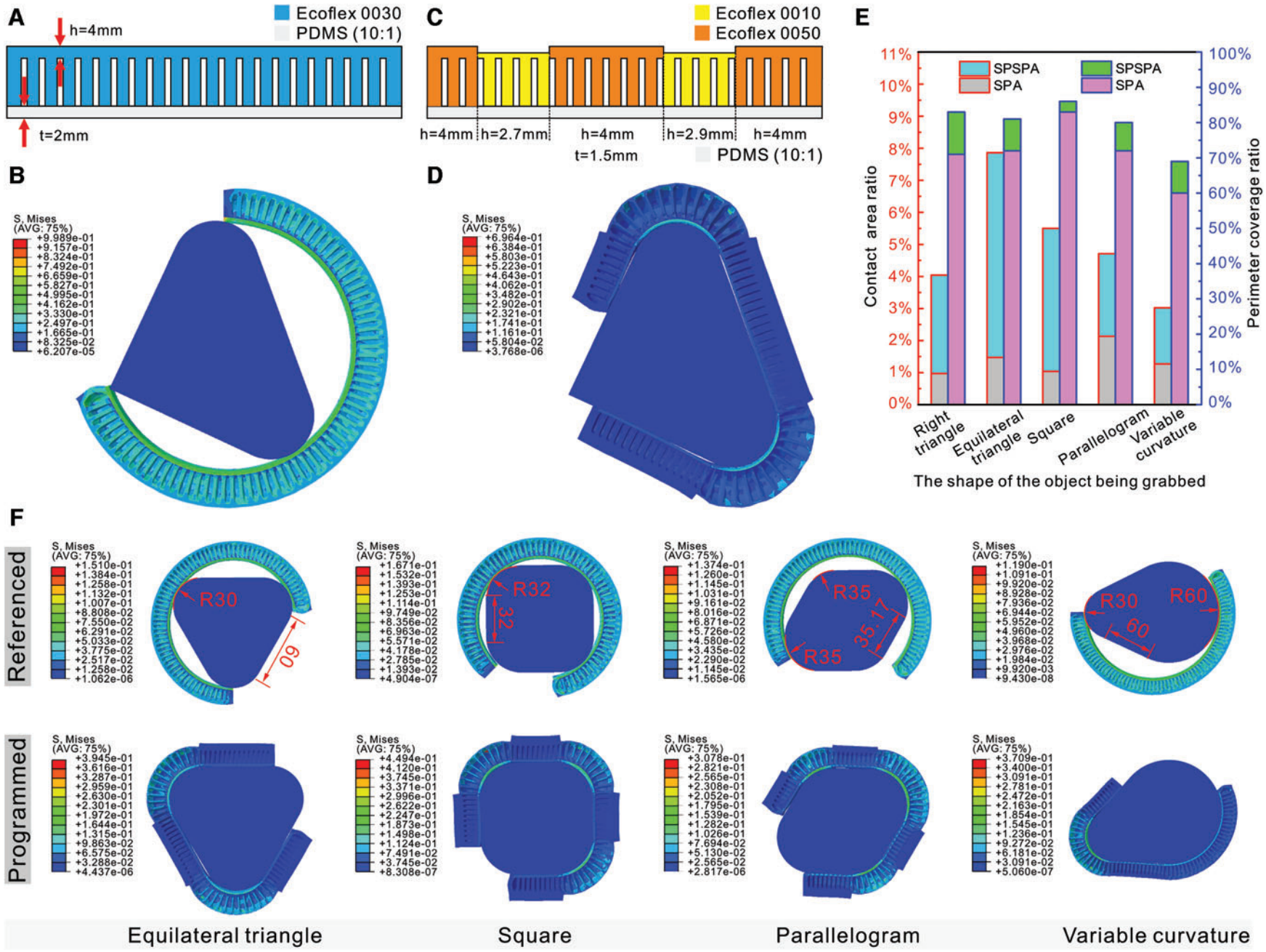

FIG. 5. Adaptability of the bending actuator. **(A–D)** The comparison of grabbing the same *right* triangle object using the dis and programmed actuator, respectively. **(E)** The adaptability comparisons of the SPSPA and the referenced SPA grabbing different shaped objects. **(F)** The simulation comparisons of the other four shapes. Color images are available online.

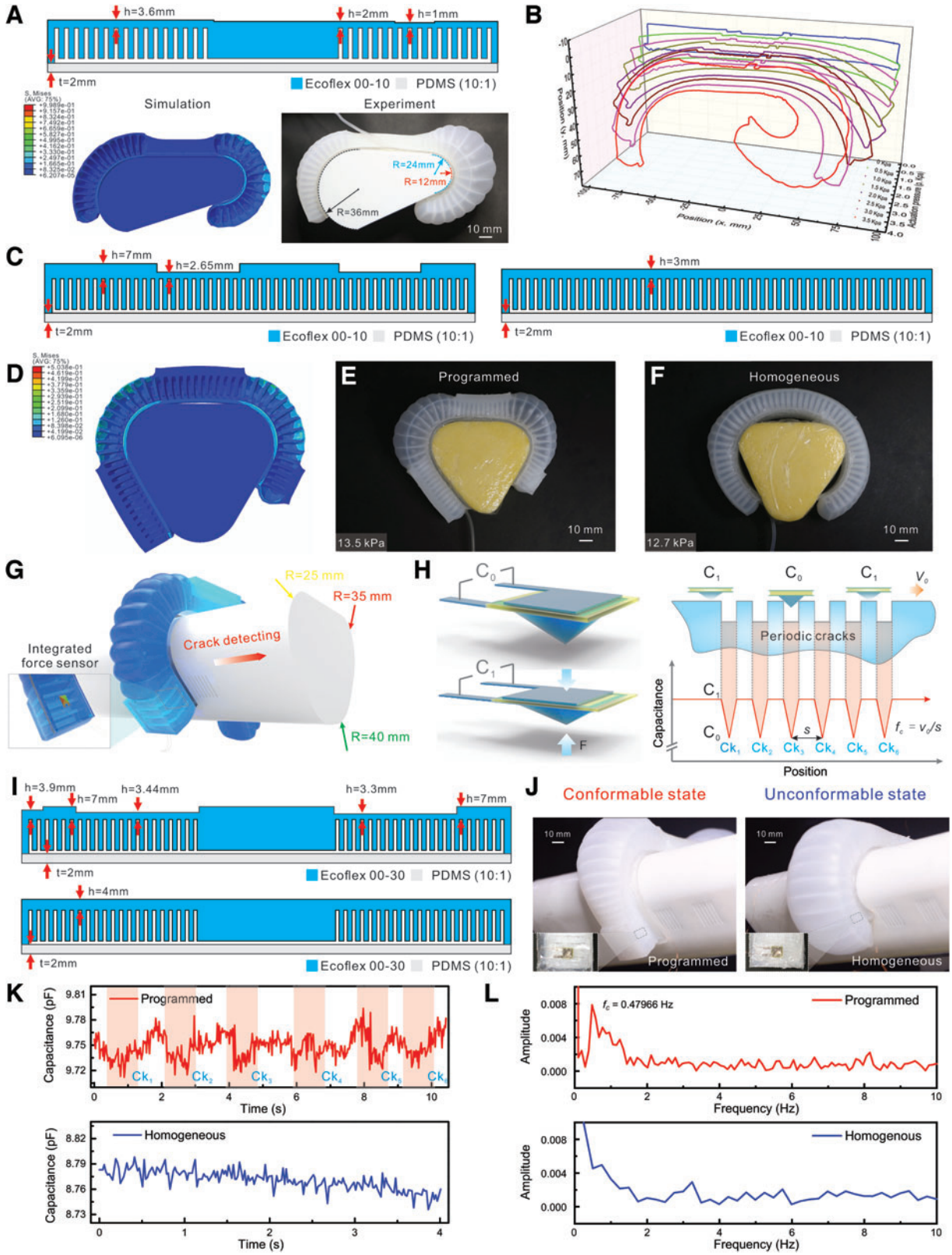

FIG. 6. Conformability demonstrations of the preprogrammed soft actuator. **(A)** Conformably grabbing a varied curvature object with an SPSPA (∼3.1 kPa). **(B)** The response cross-section profiles of the SPSPA under varied actuation pressure. **(C)** The structural design of the preprogrammed actuator and reference one, respectively. **(D)** Simulation result of the preprogrammed actuator grabbing a triangular-like cake. **(E, F)** Experimental results of grabbing a triangular-like cake by a preprogrammed and a referenced actuator, respectively. **(G)** Crack detection by a bending actuator integrated with a force sensor through contact scanning. **(H)** Sensing principles of piezocapacitive sensor with pyramidal structure toward periodic cracks. **(I)** Two structural designs of preprogrammed actuator and homogeneous actuator. **(J)** Conformal state comparisons during crack detection. **(K)** Sensing signal comparisons of two actuators scanning through cracks. **(L)** Fast Fourier Transformation of the obtained capacitive signals. Color images are available online.

actuators (detailed design of piezocapacitance sensor is in Supplementary Fig. S5). As shown in Figure 6H, in principle, when the sensor passes through the cracks, a signal change will appear due to varying normal force. Based on this principle, two actuators (programmed and homogeneous) were employed for cracking detecting (Fig. 6I). Due to the distinct conformal states, the programmed actuator provides a conformal interactive interface for the contacting sensor, whereas the homogeneous one leads to a mismatch in the sensing interface (Fig. 6J). In contrast, the SPSPA can detect surface cracks by showing a periodic jump signal marked in red in Figure 6K, whereas the homogeneous one only shows some noise signal because of the mismatched interactive interface (Supplementary Video S3). In addition, after Fourier transform, the programed one showed a characteristic frequency of $f_c = 0.48$ Hz (Fig. 6L).

Application demonstration

Conformal and high-efficient operation can empower robots with better interaction and capability. To further explore and verify the applications of SPSPAs in the soft robots, a soft pneumatic crawling robot designed with SPSPAs was constructed and crawled on a varying curvature scenario (Fig. 7A). Meanwhile, a homogeneous robot was also constructed. Figure 7B shows the detailed design of two embracing legs of the stiffness preprogrammed robot and homogeneous robot, respectively. The embracing states of two robots on the varying curvature object are shown in Figure 7C and D. Apparently, the former can achieve a better grasping because of customized stiffness distribution. Based on these two crawling robots, the kinematic and kinetic characteristics have been tested. As shown in Figure 7E–G and Supplementary Video S4, the preprogrammed robot can produce a larger pull force compared with the referenced one and achieve higher motion velocity in such a varying curvature scenario. Due to fabrication error and state difference during crawling, it is hard to guarantee each step at the same elongation of the telescopic actuator of the two robots in the experiment. Here, a correction factor (k_c) was introduced to compensate this difference for fairer comparison (the detailed method is in Supplementary Data). The corresponding actuation mechanism and detailed mold design are shown in Supplementary Figures S6 and S7, respectively.

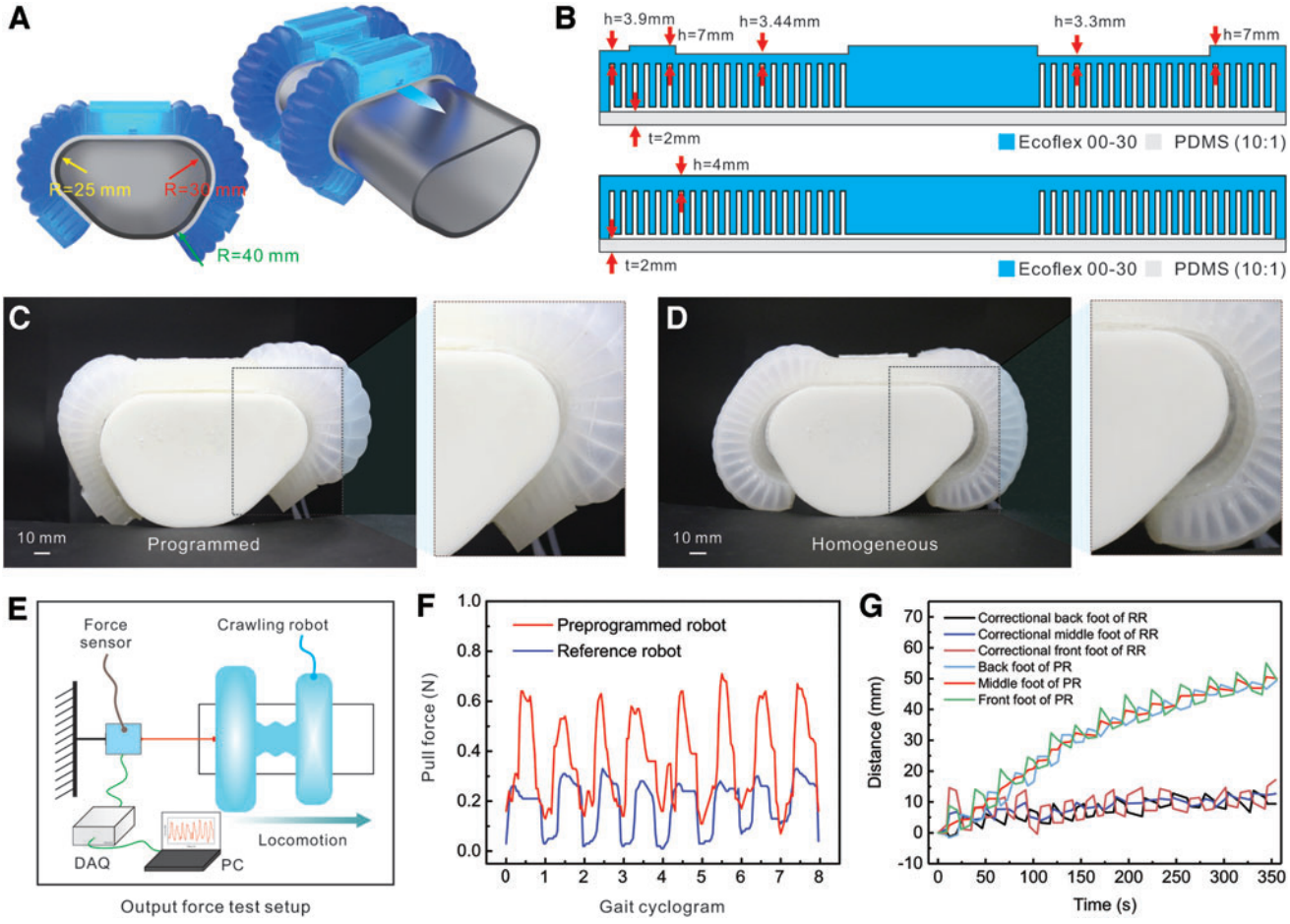

FIG. 7. Response characteristics of a soft programmed crawling robot and a referenced crawling robot. **(A)** The schematic of a robot crawling on a varying curvature object. **(B)** The structure design of the preprogrammed and referenced robot. **(C, D)** Conformal comparisons of robots with SPSPAs and homogeneous actuators. **(E)** Output force test setup for two crawling robots. **(F)** Pull force comparisons of two crawling robots on the varying curvature object in each gait cycle ($\sim$16 kPa actuated pressure for the preprogrammed robot, $\sim$18 kPa actuated pressure for homogeneous robot). **(G)** Crawling speed comparison of two robots (RR: reference robot; PR: preprogrammed robot) on a varying curvature object, and the locomotion of RR has been corrected according to the difference of elongation of two robots. Color images are available online.

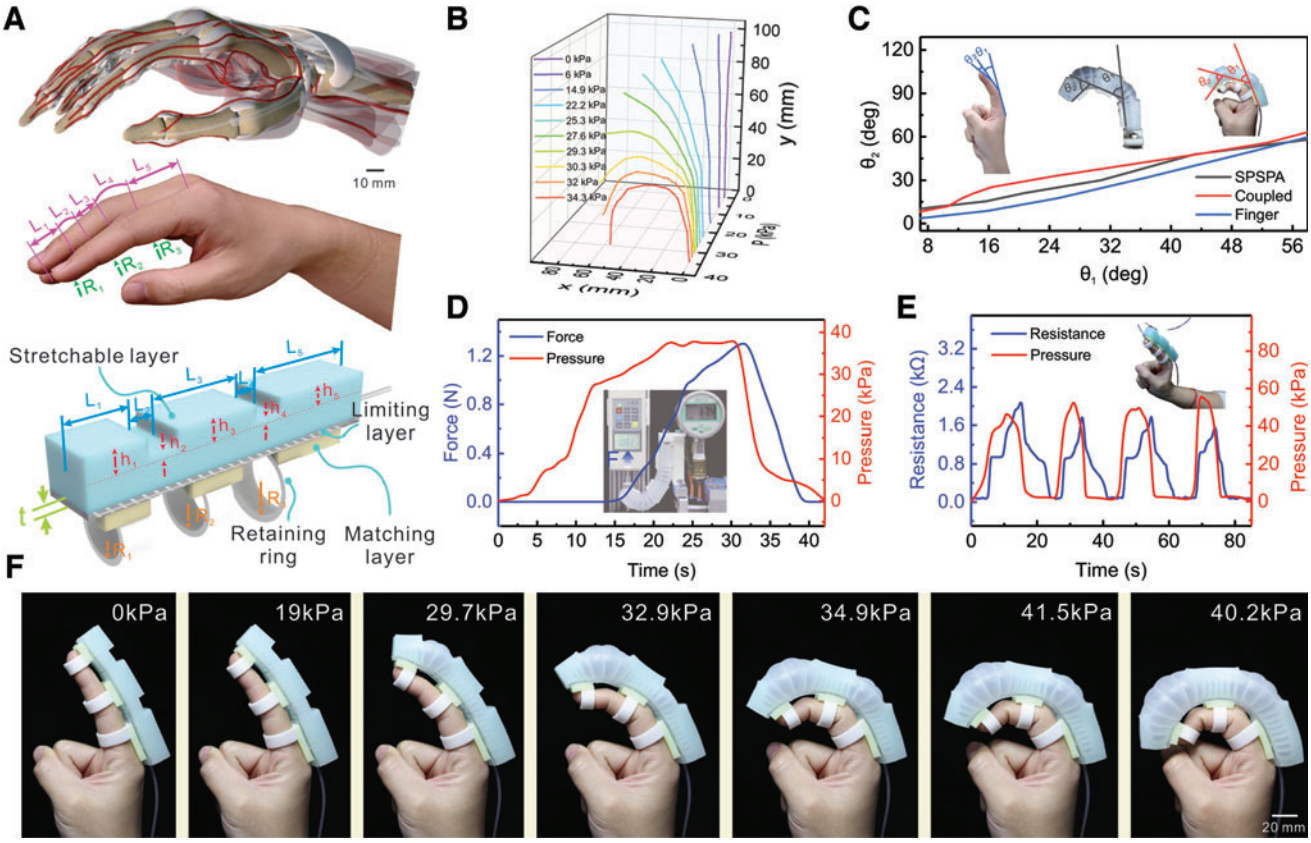

FIG. 8. SPSPA for finger rehabilitation training. **(A)** Anatomy of a human hand and the design of FR-SPSPA. **(B)** Profiles of FR-SPSPA under quasi-static actuation. **(C)** Relations between θ_1 and θ_2 of the FR-SPSPA, finger and coupled system. **(D)** Force output at the end of FR-SPSPA during actuation. **(E)** Monitoring the force FR-SPSPA exerted on the fingertip with a commercial film sensor. **(F)** Actuation process of FR-SPSPA. FR-SPSPA, finger rehabilitation SPSPA. Color images are available online.

The SPSPAs also show its advantages in rehabilitation training. A typical anatomy of finger was illustrated in Figure 8A. Based on the configuration and dimensions of index finger of patient, a customized FR-SPSPA was designed for motion rehabilitation (detailed design method and corresponding parameters are shown in Supplementary Data, Supplementary Fig. S8 and Supplementary Tables S3 and S4). Profiles of FR-SPSPA under quasi-static actuation are plotted in Figure 8B (experiment details are shown in Supplementary Data and Supplementary Fig. S9), and whole FR-SPSPA can achieve an addressable morphing with a single actuated chamber. Via an appropriate design, this underactuated FR-SPSPA can mimic well the coupled bending motion of fingers. To quantify this coupled relationship of knuckles, two angles θ_1 and θ_2 were defined (Fig. 8C). The behavior of FR-SPSPA is consistent with that of a finger. One joint bends in proportion to the other. Consequently, when the FR-SPSPA is mounted on the finger, two joints also behave linearly. These three curves (SPSPA, coupled and finger) are close to each other, suggesting that the FR-SPSPA matches well with the natural motions of finger. Dynamic characteristics of this FR-SPSPA are quantified in Figure 8D and E. The distal output force of this FR-SPSPA was characterized in Figure 8D. The peak output force can reach 1.2 N when air pressure rises to ~40 kPa, which is enough for driving the motion of fingers in relaxed states. In addition, the whole rehabilitation training process can be monitored with a piezoresistance sensor mounted on a retaining ring (detailed characterization of the sensor is in Supplementary Data and Supplementary Fig. S10) (Fig. 8E). Benefiting from the nature of soft materials and the customized stiffness (Supplementary Data and Supplementary Fig. S11), FR-SPSPA can interact safely and steadily with the finger. It provides a comfortable rehabilitation training with an addressable and conformal motion, as depicted in Figure 8F and Supplementary Video S5. In addition, several soft pneumatic crawling robots in unstructured scenarios were demonstrated (Supplementary Data and Supplementary Fig. S12 and Video S6).

Conclusions

In brief, we present a facile method to encode stiffness profiles in classical SPAs via selectively preprogramming mechanically gradient structure and materials. Further, a targeted shape predication model related with critical structural and material parameters is built, which enables a reversal solution of designed parameters (Supplementary Data and Supplementary Fig. S13). Based on the presented stiffness preprogrammable design method, several SPSPAs have been tailored for curvature varying scenarios, showing addressable bending behaviors. This design method enables adaptive operation and interaction of soft actuators in some specific scenarios, such as conformal grasping, contact sensing, and finger rehabilitation. Further, this stiffness preprogrammable method can also empower soft robots with better kinetic and kinematic

characteristics and simplify the control complexity without additional independent actuation chambers to achieve addressable actuation. This method can serve as a useful way to customize soft robots in many specific-purposed, single, and repetitive application scenarios where varying curvature, conformal and efficient interaction are needed. It may pave a new way for future applications of soft robots in precise and gentle operations, contacting sensing, and human–machine interaction, for example, gentle rehabilitation and assistive human–machine interaction, conformal sensing, and compatible manipulation of tender objects.

Author Contributions

Z.W. and X.K. conceived the concept. X.K. and Z.C. performed the simulations. X.K., Z.C., J.J., H.Y., J.Z., and H.C. carried out the experiments and data processing, X.K. Z.W. drafted the article. X.K. Z.C., H.Y., C.F.G., Z.W., and H.D. analyzed the data and interpreted the results. Z.W. and H.D. directed the project. All authors commented on the article.

Author Disclosure Statement

No competing financial interests exist.

Funding Information

The materials based on the work were partly financially supported by the National Natural Science Foundation of China (Grant No. U1613204, L1924046) and the National Key R&D program of China (Grant No. 2017YFB1303100).

Supplementary Material

Supplementary Data
Supplementary Figure S1
Supplementary Figure S2
Supplementary Figure S3
Supplementary Figure S4
Supplementary Figure S5
Supplementary Figure S6
Supplementary Figure S7
Supplementary Figure S8
Supplementary Figure S9
Supplementary Figure S10
Supplementary Figure S11
Supplementary Figure S12
Supplementary Figure S13
Supplementary Table S1
Supplementary Table S2
Supplementary Table S3
Supplementary Table S4
Supplementary Table S5
Supplementary Video S1
Supplementary Video S2
Supplementary Video S3
Supplementary Video S4
Supplementary Video S5
Supplementary Video S6

References

1. Shepherd RF, Ilievski F, Choi W, *et al.* Multigait soft robot. Proc Natl Acad Sci U S A 2011;108:20400–20403.
2. Lee C, Kim M, Kim YJ, *et al.* Soft robot review. Int J Control Autom Syst 2017;15:3–15.
3. Rich SI, Wood RJ, Majidi C. Untethered soft robotics. Nat Electron 2018;1:102–112.
4. Hines L, Petersen K, Lum GZ, *et al.* Soft actuators for small-scale robotics. Adv Mater 2017;29:1603483.
5. Kim S, Laschi C, Trimmer B. Soft robotics: a bioinspired evolution in robotics. Trends Biotechnol 2013;31:287–294.
6. Rus D, Tolley MT. Design, fabrication and control of soft robots. Nature 2015;521:467–475.
7. Cianchetti M, Laschi C, Menciassi A, *et al.* Biomedical applications of soft robotics. Nat Rev Mater 2018;3:143–153.
8. Hawkes EW, Blumenschein LH, Greer JD, *et al.* A soft robot that navigates its environment through growth. Sci Robot 2017;2:eaan3028.
9. Wang Y, Yang X, Chen Y, *et al.* A biorobotic adhesive disc for underwater hitchhiking inspired by the remora sucker-fish. Sci Robot 2017;2:eaan8072.
10. Morin SA, Shepherd RF, Kwok SW, *et al.* Camouflage and display for soft machines. Science (80-.) 2012;337:828–832.
11. Li T, Li G, Liang Y, *et al.* Fast-moving soft electronic fish. Sci Adv 2017;3:e1602045.
12. Gu G, Zou J, Zhao R, *et al.* Soft wall-climbing robots. Sci Robot 2018;3:eaat2874.
13. Nelson BJ, Kaliakatsos IK, Abbott JJ. Microrobots for minimally invasive medicine. Annu Rev Biomed Eng 2010; 12:55–85.
14. Chiaradia D, Xiloyannis M, Antuvan CW, *et al.* Design and embedded control of a soft elbow exosuit. 2018 IEEE International Conference on Soft Robotics, Livorno, Italy. IEEE 2018:565–571.
15. Tottori S, Zhang L, Qiu F, *et al.* Magnetic helical micromachines: fabrication, controlled swimming, and cargo transport. Adv Mater 2012;24:811–816.
16. Li S, Batra R, Brown D, *et al.* Particle robotics based on statistical mechanics of loosely coupled components. Nature 2019;567:361–365.
17. Byrne O, Coulter F, Glynn M, *et al.* Additive manufacture of composite soft pneumatic actuators. Soft Robot 2018;5: 726–736.
18. Martinez RV, Fish CR, Chen X, *et al.* Elastomeric origami: programmable paper-elastomer composites as pneumatic actuators. Adv Funct Mater 2012;22:1376–1384.
19. Usevitch NS, Okamura AM, Hawkes EW. APAM: antagonistic pneumatic artificial muscle. 2018 IEEE Int Conf Robot Autom 2018;1539–1546.
20. Terryn S, Brancart J, Lefeber D, *et al.* Self-healing soft pneumatic robots. Sci Robot 2017;2:eaan4268.
21. Laschi C, Mazzolai B, Cianchetti M. Soft robotics: technologies and systems pushing the boundaries of robot abilities. Sci Robot 2016;1:eaah3690.
22. Verma MS, Ainla A, Yang D, *et al.* A soft tube-climbing robot. Soft Robot 2018;5:133–137.
23. Schaffner M, Faber JA, Pianegonda L, *et al.* 3D printing of robotic soft actuators with programmable bioinspired architectures. Nat Commun 2018;9:878.
24. Hoang TT, Phan PT, Thai MT, *et al.* Bio-inspired conformable and helical soft fabric gripper with variable stiffness and touch sensing. Adv Mater Technol 2020;5:1–14.
25. Connolly F, Polygerinos P, Walsh CJ, *et al.* mechanical programming of soft actuators by varying fiber angle. Soft Robot 2015;2:26–32.

26. Sun Y, Yap HK, Liang X, *et al.* Stiffness customization and patterning for property modulation of silicone-based soft pneumatic actuators. Soft Robot 2017;4:251–260.
27. Jiang Y, Chen D, Liu C, *et al.* Chain-like granular jamming: a novel stiffness-programmable mechanism for soft robotics. Soft Robot 2019;6:118–132.
28. Lum GZ, Ye Z, Dong X, *et al.* Shape-programmable magnetic soft matter. Proc Natl Acad Sci U S A 2016;113: E6007–E6015.
29. Wang Q, Tian X, Huang L, *et al.* Programmable morphing composites with embedded continuous fibers by 4D printing. Mater Des 2018;155:404–413.
30. Qi S, Guo H, Fu J, *et al.* 3D printed shape-programmable magneto-active soft matter for biomimetic applications. Compos Sci Technol 2020;188:107973.
31. Kuang X, Wu J, Chen K, *et al.* Grayscale digital light processing 3D printing for highly functionally graded materials. Sci Adv 2019;5:eaav5790.
32. Lee H, Jang Y, Choe JK, *et al.* 3D-printed programmable tensegrity for soft robotics. Sci Robot 2020;5: eaay9024.
33. Dudte LH, Vouga E, Tachi T, *et al.* Programming curvature using origami tessellations. Nat Mater 2016;15:583–588.
34. Jeong SH, Zhang S, Hjort K, *et al.* PDMS-based elastomer tuned soft, stretchable, and sticky for epidermal electronics. Adv Mater 2016;28:5830–5836.
35. Wu Z, Zhang S, Vorobyev A, *et al.* Seamless modulus gradient structures for highly resilient, stretchable system integration. Mater Today Phys 2018;4:28–35.
36. Polygerinos P, Wang Z, Overvelde JTB, *et al.* Modeling of soft fiber-reinforced bending actuators. IEEE Trans Robot 2015;31:778–789.

Address correspondence to:
Zhigang Wu
State Key Laboratory of Digital Manufacturing Equipment and Technology
Huazhong University of Science and Technology
Wuhan 430074
China

E-mail: zgwu@hust.edu.cn